Manipulating optical reflections using engineered nanoscale metasurfaces

Nasim Mohammadi Estakhri and Andrea Alù

Department of Electrical and Computer Engineering, The University of Texas at Austin, Austin, Texas 78712, USA
(Received 7 March 2014; revised manuscript received 15 May 2014; published 16 June 2014)

We propose a comprehensive scheme for the efficient design of graded optical metasurfaces capable of rerouting the impinging energy at will in a flexible way. We show that carefully designed conjoined optical nanoelements may be used as basic building blocks to arbitrarily shape the reflected phase front, while providing large controllability and low loss over deeply subwavelength thicknesses. The metasurface elements are designed using transmission line concepts combined with nanocircuit theory, and they can be realized with conventional lithographic techniques. Based on these concepts, we put forward a fast and accurate analytical model to design the optical analog of reflectarrays for light bending, steering, and focusing. The proposed designs show large efficiency over a broad angular spectrum, accompanied by broad bandwidths of operation. Our technique may lead to significant advances in the field of planarized nanophotonics and light manipulation over a surface, with potential applications in light trapping and efficient photonic couplers.

I. INTRODUCTION

While it is an important challenge to be able to arbitrarily control and shape the propagation of light, recent advances in nanofabrication techniques have pushed forward the quest for efficient light management at the nanoscale. One of the challenging aspects in this context is to achieve full control, with subwavelength resolution, on the local phase and amplitude of the optical wave as it interacts and emerges from a thin device, which may enable tailoring the wave front in an arbitrary desired way. Conventional optical devices, such as dielectric lenses and prisms, offer a convenient solution to control light, based on the accumulation of phase as the wave propagates inside them. However, on account of the limited range of permittivity and permeability of natural materials, these devices are often bulky and inappropriate for direct integration into nanophotonic systems. The unprecedented capabilities of artificially engineered structures, known as metamaterials, have recently allowed an elegant solution to these natural constraints. Rather than merely relying on the electromagnetic response of atoms in bulk media, collections of carefully designed nanostructures may realize effective properties, appropriate for a wide range of applications, including negative refraction, subwavelength imaging, and invisibility cloaks [1–8].

Three-dimensional (3D) metamaterials have been shown to offer significant flexibility in terms of design and functionality, but their complicated fabrication along with inherently large losses around the frequency of interest usually challenge their performance [9]. For this reason, two-dimensional (2D) geometries, usually referred to as metasurfaces, have attracted significant attention in recent years [10–13]. These structures are compact and low profile and offer several new functionalities; in addition, they can be directly integrated into nanophotonic systems and exhibit moderate insertion loss as a result of wave-matter interaction over ultrathin thicknesses. Such unique properties, along with their compatibility with the current lithographic techniques, have propelled their use in a wide range of applications (see, e.g., Refs. [10,11]). Metasurfaces have raised significant attention thanks to the recently proposed generalized Snell's law of reflection and refraction, based on which an interesting scheme to control wave propagation was put forward according to properly designed gradient of phase discontinuity over a subwavelength surface [14–17]. The possibility of locally controlling the light flow over a surface brings up several applications in optics and photonics and ascertains a promising future for metasurfaces, which may become an interesting alternative for 3D metamaterials. These first proposals were, however, characterized by a number of limitations, including polarization sensitivity and low efficiency [14–16,18]. Another major barrier to the efficient use of these concepts, especially at shorter wavelengths, resides in the difficulty to arbitrarily imprint the desired impedance or phase pattern over an ultrathin surface.

In this paper, motivated by the mentioned challenges and potential applications of this concept, we describe in detail an alternative solution to design graded metasurfaces based on the nanocircuit paradigm [19]. Inspired by the broad literature on reflectarrays, we extend the concept of impedance surface design from radio frequency and midinfrared regimes [14,20,21], into the visible range using conjoined optical nanoelements as novel compact impedance blocks with scalable properties. We show that such a configuration can inherently perform as a controllable, deeply subwavelength phase element, realizing subwavelength circuit components at optical frequencies that can control, to a large degree, any reflected beam profile. We provide a comprehensive analysis and discussion on the performance of the proposed configuration along with some device examples implemented, based on this concept.

II. THEORETICAL RESULTS AND DISCUSSION

When an electromagnetic wave interacts with a metasurface that holds a transversely inhomogeneous profile, an additional momentum can be locally imposed on the impinging wave due to its space gradient [14]. Such a thin metasurface may be accurately modeled as an effective impedance sheet with inhomogeneous surface reactance, suitably tailored to locally control the local phase imparted to the reflected or transmitted waves. However, the phase range available with a single surface is strictly limited by fundamental passivity requirements [22].

Polarization mixing may be used to overcome these limits, as originally proposed in [14], but this comes at the price of large inefficiencies. At lower frequencies, a viable alternative is provided by the use of magnetic currents, which, in return, require a finite thickness of the metasurface, but can provide full control over the imparted phase [23]. This approach is not necessarily easily scalable to optical frequencies.

Recently, we put forward the concept of meta-transmitarrays as a general solution to circumvent these limitations, based on a symmetric stack of three metasurfaces with a transverse inhomogeneous profile [22]. The proposed configuration enables full control on the amplitude and phase of the transmitted wave through precise engineering of the reactance of each surface. We have shown that any intended phase profile $\varphi(\vec{r})$ may be imprinted on the transmitted wave, while efficient transmission is guaranteed, provided that each of the three metasurfaces holds the normalized reactance profile

$$X_{1,3}(\vec{r}) = -\frac{\sin(D)\sin(\varphi(\vec{r})/2)}{\sin(D + \varphi(\vec{r})/2)},$$

$$X_2(\vec{r}) = -\frac{\sin(D)^2}{\sin(2D) + \sin(\varphi(\vec{r}))}, \tag{1}$$

where $\vec{r}$ shows the transverse variation over the structure, D is the electrical distance between plates, and X_n, with $n = 1,2,3$, is the reactance profile of the nth metasurface in the order in which they are stacked. While this setup is conceptually interesting, realizing three stacked metasurfaces with controlled transverse inhomogeneities and a subwavelength alignment may be challenging in practice.

For this reason, in the following, we discuss an alternative setup aimed at manipulating the reflected wave, rather than the transmitted one. The proposed meta-reflectarrays can provide ultimate control of the profile of the reflected optical wave with subwavelength resolution. Figure 1 shows an example of the reflectarray configuration, with its fundamental building block [Fig. 1(a)] and its overall geometry [Fig. 1(b)]. In this configuration, the desired phase $\varphi(\vec{r})$ may be imprinted on the reflected wave, employing a single metasurface, thanks

to the imaging properties of the back reflector. In a local sense, the phase discontinuity $\varphi(\vec{r})$ at each point on the surface is directly related to the normalized reactance $X(\vec{r})$, using a simple transmission line model analogous to the lower panel of Fig. 1(a), at each point. The laterally inhomogeneous surface reactance is then related to the local phase as

$$X(\vec{r}) = \frac{1}{-n_{\text{sub}}\cot(D) + \tan(\varphi(\vec{r})/2)}. \tag{2}$$

Here, n_{sub} and D are the substrate refractive index and electrical thickness, respectively. Equation (2) is generally valid for arbitrary $\varphi(\vec{r})$, and it shows that we may be able to efficiently imprint any arbitrary phase distribution on the reflected wave by means of a suitable reactance management. This may include linear phase variation along the surface to realize anomalous beam-steering or quadratic phase profiles to create ultrathin flat lenses. The variation on the phase profile should be able to supply a full control over the 2π range and may be imparted on the surface after proper discretization, provided that each discrete element, as in Fig. 1(a), is sufficiently small compared to the wavelength for the application of interest. The proposed geometry translates the reflectarray concepts to optical frequencies and takes advantage of the nanocircuit concepts and the plasmonic features of metals in the visible range to squeeze down the dimensions of the building blocks to the nanometer scale, with relevant advantages in terms of subwavelength control on the reflected signal. These possibilities open unprecedented flexibility to manipulate the optical beam for numerous applications, some of which are described in the following sections.

A. Deeply subwavelength spatial phase modulators

The critical challenge to apply the proposed concept at optical frequencies is the design of deeply subwavelength nanocircuit elements that can span the whole required reactance variation described in Eqs. (1) and (2). In the microwave regime, several configurations have been proposed to synthesize arbitrary impedance profiles over a surface. These designs typically exploit resonant patch antennas [24,25] or
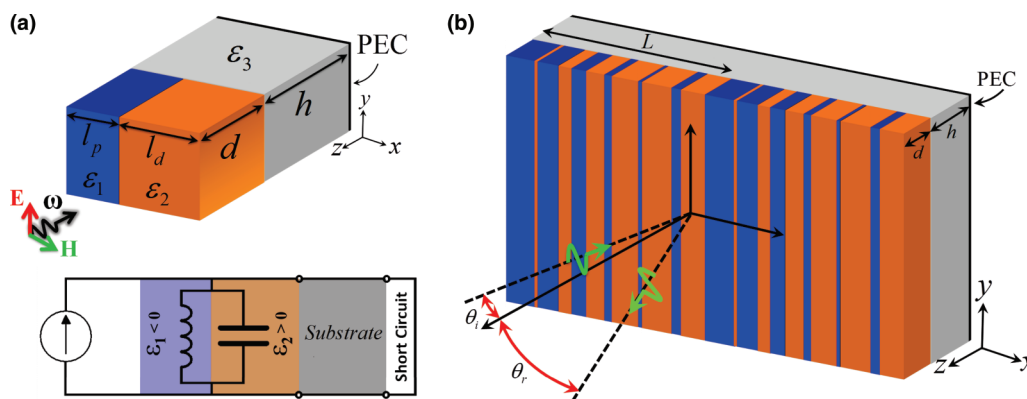

FIG. 1. (Color online) Subwavelength spatial phase modulator. (a) Upper panel: fundamental building block of the proposed metareflector, a nanoresonator made of plasmonic (blue) and dielectric (orange) materials, deposited on a substrate (gray) and backed by a ground plane reflector. Lower panel: equivalent circuit and transmission line model describing the quasistatic behavior of the proposed configuration. Metasurface elements are substituted by their circuit equivalents forming a lumped resonator sandwiched between two terminated transmission lines. (b) A gradient metasurface with linear phase variation along x, operating as an ultrathin beam-steering surface.

ring resonators [26]; however, the size of these elements is generally of the order of half-wavelength to support the required resonance. This property ultimately limits the maximum attainable resolution to locally control the wave reflection through a passive surface; an active design may shrink the size by up to three to four times [27]. At shorter wavelengths, however, nanometallic objects support collective electron excitations (known as plasmonic effects), providing an appealing solution for subwavelength phase management. Here, we utilize the inherent potential of plasmonic structures to squeeze resonant light interaction into subdiffractive volumes, enabling quasistatic resonances in order to realize deeply subwavelength ultrathin spatial phase modulators.

Our idea is to use LC nanoresonators, largely tunable with their aspect ratio (therefore easily and effectively controllable over small sizes), and analytically modeled in an accurate and efficient way using nanocircuit theory. To separately realize the required inductance and capacitance, we use the nanocircuit paradigm introduced in [19]. This concept, demonstrated experimentally in [28], has been extensively used for many optical designs, including antenna loading and matching [29,30], optical microscopy [31], optical filter design [32], and nanotransmission line synthesis [33]. The power of this paradigm consists in being able to translate to the nanoscale the design tools available at lower frequencies in the context of circuit theory, providing interesting possibilities in optical design and related applications [34]. The optical lumped impedance is generally defined based on the displacement current flowing through each element, and the material choice directly determines the type of circuit component that each particle constitutes. Specifically, the sign of permittivity at the frequency of interest determines whether a nanocapacitor ($\mathrm{Re}[\varepsilon] > 0$) or nanoinductor ($\mathrm{Re}[\varepsilon] < 0$) is formed. Material loss directly translates into nanoresistance in the circuit element, which, if properly controlled, may also allow locally tailoring the amplitude of the emerging beam. The effective impedance of each element primarily depends on the field distribution inside its volume. For instance, the effective impedance of a homogeneous nanoblock, as in Fig. 1, equals $Z = \frac{H}{j\omega \varepsilon S}$, where H and S are the height, parallel to the electric field, and the surface area normal to it, respectively [35].

Accordingly, the proposed LC nanoelement is shown in Fig. 1(a), and it is composed of a conjoined nanoparticle formed by a plasmonic portion with negative permittivity and a dielectric portion with positive permittivity, forming a shunt LC connection when the electric field is parallel to the common interface of the two materials. As suggested by Eqs. (1) and (2), if we are able to arbitrarily shape the surface impedance, a single reflecting metasurface or three stacked metasurfaces in a transmitting scenario can guarantee complete control of the reflection or transmission phase and amplitude simultaneously. Our concern here is to keep the size of each element deeply subwavelength, i.e., $l = l_p + l_d \ll \lambda_0$, in which l_p is the length of plasmonic portion and l_d is the length of dielectric portion, as indicated in Fig. 1(a). For the moment, let us assume a one-dimensional variation over the surface, which implies that Fig. 1(a) represents a 2D element, with unit length impedance in the y direction and period l in the x direction. An incident

monochromatic plane wave with electric field $\mathrm{E}_0 = \mathrm{E}_0 \hat{y}$ is assumed to illuminate the surface at normal incidence, with an $e^{j\omega t}$ time variation. To meet our resolution requirements, the element size is chosen to be as small as $l = \lambda_0/16$, where $\lambda_0 = 500$ nm is the center design wavelength [36]. We choose silver as the plasmonic material, due to its relatively low loss, while for the nanocapacitor, we choose a high-index dielectric with permittivity $\varepsilon_2 = 12\varepsilon_0$: AlAs [37]. At optical frequencies, silver is modeled with a Drude-type permittivity as $\varepsilon_1 = \varepsilon_\infty - \omega_p^2/\omega(\omega - j\gamma)$, with $\varepsilon_\infty = 5$, $\omega_p/2\pi = 2175$ THz and $\gamma/2\pi = 4.35$ THz, based on experimental measurement data, taking into account the realistic loss and frequency dispersion [38]. The considered realistic losses in our example translate into lossy circuit elements in the equivalent circuit model of Fig. 1(a). Nanocircuit theory can be used to estimate the local effective impedance provided by this unit cell, which corresponds to the circuit model in Fig. 1(a) and equals $Z_{\mathrm{eff}} = Z_1 \| Z_2$, where Z_1 and Z_2 are the corresponding impedance of each element, given by $Z_{1,2} \approx (j\omega l_{p,d}(\varepsilon_{1,2} - \varepsilon_0)d)^{-1}$. By changing the filling ratio of the proposed nanoblock, we can achieve a strong spatial modulation of the local surface reactance.

The reflection phase from a periodic metasurface formed by an array of unit cells, as in Fig. 1(a), may be analytically calculated as a function of the filling ratio, as shown in Fig. 2(a). In this example, the thickness of the metasurface is set at $d = 40$ nm $= 0.08\lambda_0$, justifying the impedance sheet approximation, and it is backed by a metallic mirror with a $h = 100$ nm spacing. By sweeping the filling ratio of the nanoblock, we move from a capacitive to an inductive surface. For a specific filling ratio, the nanocapacitor and nanoinductor form a deeply subwavelength shunt resonator, supporting a rapid variation in the reflection phase, which allows covering almost the entire 2π phase spectrum.

The strength of the proposed configuration may be appreciated by noticing that this large dynamic phase variation occurs over a $\lambda_0/16$ lateral distance, far superior to previously proposed configurations for infrared and optical metasurfaces [14,21,39]. Given the plasmonic nature of this resonance and the simple shunt combination of nanocircuit elements, this phase variation may be attained with even more deeply subwavelength unit cells. In order to further examine the validity of our model, the reflection phase from the same configuration is calculated using full-wave numerical simulations [40]. Results are compared in Fig. 2(a) (black dashed line), demonstrating an excellent agreement and opening interesting opportunities for the fast and accurate design of efficient ultrathin metasurfaces based on this concept. We show in Fig. 2(b) the reflection phase for an analogous design but with a thinner spacer between the metallic reflector and the nanocircuit elements: $h = 40$ nm. The range of the achieved phase [compared with Fig. 2(a)] is almost unchanged, as we rely on a lateral resonance, rather than on propagation effects through the substrate.

Embedding the proposed subwavelength phase modules in an inhomogeneous optical metasurface can resolve the typical challenges in this frequency range associated with resolution and efficiency. However, technological limitations typically impose some additional constraints on the minimum
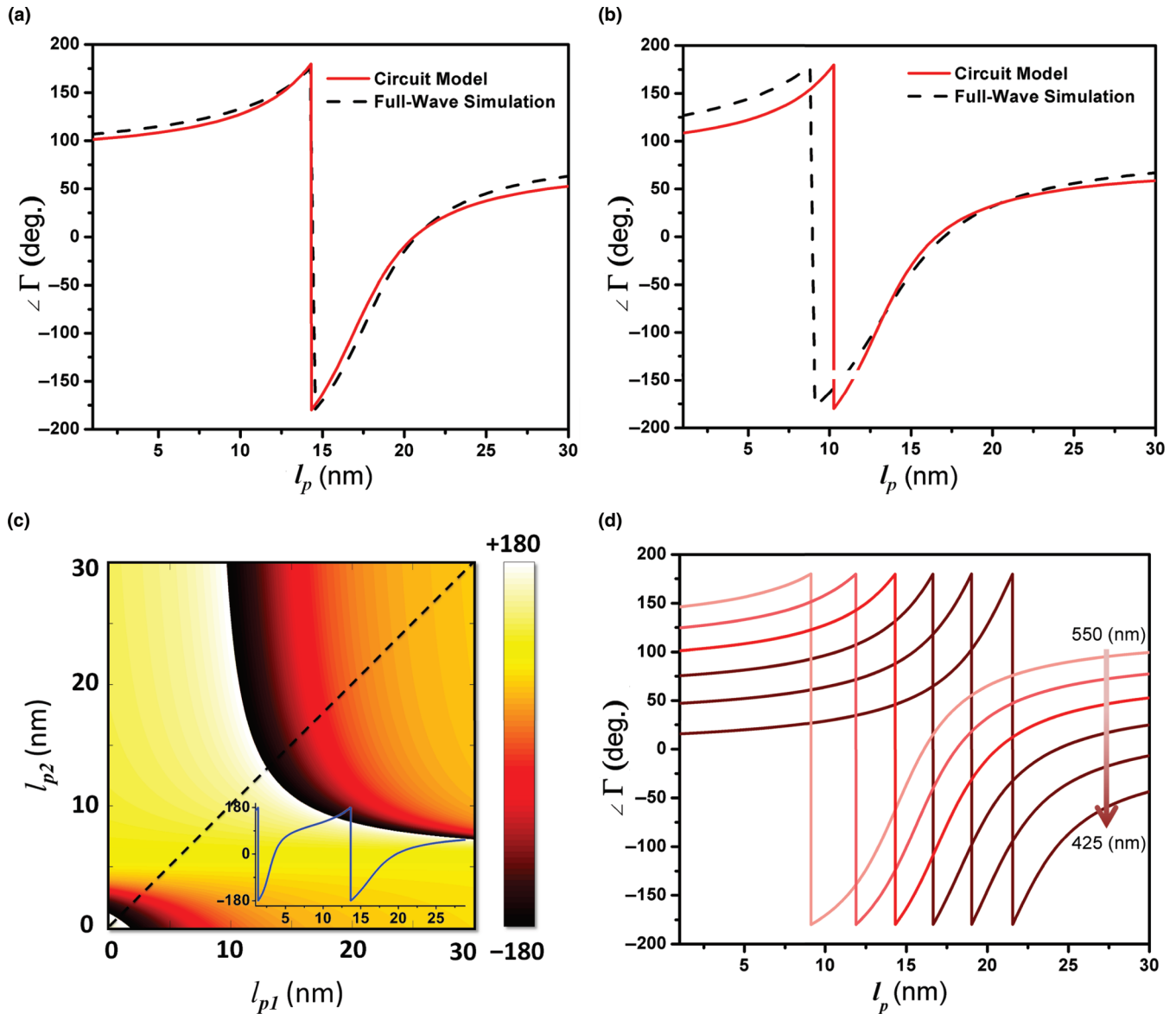
FIG. 2. (Color online) Reflection phase. (a) Reflection phase for a periodic metasurface composed of the unit cell, shown in Fig. 1(a), as a function of the width l_p. Here, $h = 100$ nm, $d = 40$ nm, and $l = l_p + l_d = 31.25$ nm. The phase is calculated at $\lambda_0 = 500$ nm using the transmission line and circuit model approach (red line) and full-wave numerical simulations (black dashed line). (b) Same as in (a), when the metasurface is positioned at $h = 40$ nm from the back plane. (c) Reflection phase from a dual-layer metasurface with each layer analogous to Fig. 1(a). The phase variation is plotted as function of l_{p1} and l_{p2}, widths of the plasmonic portion in the two layers, for $h = d = 30$ nm and $l = 31.25$ nm. The inset shows the phase variation along the symmetry line, i.e., for $l_{p1} = l_{p2}$. (d) Evolution of the reflection phase as a function of wavelength. The metasurface is the same as (a), and the reflection phase is calculated over the range $\lambda = 425$ nm (dark red) to $\lambda = 550$ nm (light red). Constitutive materials are Ag and AlAs. All phases are calculated at a plane 300 nm above the metasurface.

resolution of the spatial phase modulator and eventually determine the overall performance of the device. One way to overcome these limitations at high frequencies is to use multiple stacked surfaces, which may add further degrees of freedom in selecting the device dimensions. Along this line, Fig. 2(c) shows the reflection phase variation for a double-layer periodic metasurface for which each layer is composed of the same design as in Fig. 1(a). The layers are identical in terms of thickness and spacing, but each can have its own filling ratio. It is seen that the filling ratios may be chosen with large degrees of freedom to meet the technological limitations and avoid fine features. The size of the building blocks may also

be increased to reduce the manufacturing difficulties typically associated with shorter wavelengths.

B. A plasmonic meta-reflectarray

The possibility to induce an arbitrary reflection phase pattern with subwavelength resolution suggests several exciting venues for applications of the proposed optical meta-reflectarrays. These metasurfaces may offer an efficient way to steer the direction of the reflected plane wave without employing mechanically rotated mirrors. This is consistent with the way that reflectarrays and transmitarrays operate
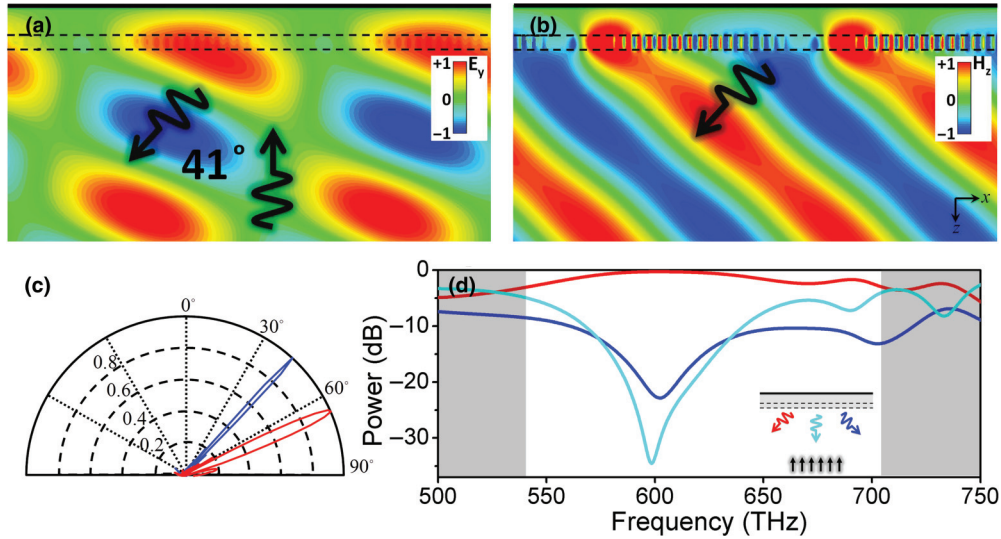
FIG. 3. (Color online) Light-bending and bandwidth characteristics. (a) Electric field and (b) magnetic field distribution (snapshot in time) under normal incidence for the geometry in Fig. 1(b), designed to tilt the impinging wave by 41° towards the negative x axis. Fields are plotted in the transverse plane (xz plane) and illustrate interference and reflection distributions, respectively. The structure has a superlattice period of $1.5\lambda_0$, designed based on the phase data in Fig. 2(a). (c) Far-field scattering patterns for two metasurfaces, tailored to reflect a normally incident plane wave by 41° (blue) and 63° (red) off the normal. (d) Normalized reflected power toward the three dominant harmonics versus frequency for the metasurface of panel (a). A normally incident wave scatters back at 41° (red curve), −41° (blue curve), and 0° (aqua curve) at 600 THz, schematically shown in the inset. The highlighted region indicates the −3-dB operation bandwidth.

at radio frequencies but with two important advantages: the subwavelength resolution, with which this control may be attained, leads to much steeper steering angles and higher conversion efficiencies; and the possibility to translate these concepts to the visible range, which we focus on in the following.

In order to deflect the incident light into a particular direction the metasurface must provide a constant phase gradient along the desired path, as in Fig. 1(b). For an incident wave with angle θ_i to be redirected toward the angle θ_r upon reflection, the phase function imparted by the surface must follow a linear distribution $\varphi(x) = \alpha x$, where $\pm\alpha = k_0 \sin\theta_r - k_0 \sin\theta_i$ and k_0 is the free-space wave number. The sign of α indicates whether the incident wave experiences a negative or positive shift in the reflection angle, and the final structure becomes periodic with a superlattice period $L = |\lambda_0/(\sin\theta_r - \sin\theta_i)|$, associated to the design wavelength of λ_0. We notice two important issues here: first, in designing the metasurface we use the design principles developed in the previous section for a periodic metasurface composed of one of the building blocks. In other words, in order to locally tailor the phase along an inhomogeneous metasurface, we assume that the mutual coupling among elements is negligible. As our full-wave simulations in the following show, and consistent with the assumption of deeply subwavelength inclusions and of a smoothly varying phase profile, this assumption is satisfied in this and all the following examples. Second, we note that the superlattice periodicity introduced here to bend the impinging beam to an arbitrary direction is not a requirement. We may synthesize the required linear phase gradient along the metasurface with a variety of different inclusions and therefore, in principle, envision a fully nonperiodic metasurface achieving the same effect. The superlattice periodicity is

introduced here to facilitate the design and realization of the structure.

Figures 3(a)–3(b) show the reflection field pattern from a graded metasurface designed to bend the normal incident wave by an angle of 41°. For this purpose, a supercell period $L = \lambda_0/\sin 41 = 1.5\lambda_0$ is required, which we fill with 24 unit cells (each with the size of $\lambda_0/16$), based on the reflection phase data previously presented in Fig. 2(a), imparting the required linear gradient of phase variation. Notice that different from Fig. 2, we now assume that the metasurface is not periodic at the unit cell level but instead has a graded variation over a $1.5\lambda_0$ period to impart the desired transverse momentum in reflection. As predicted, the phase of the reflected wave is shifted by the reactance gradient, and a normally incident wave is efficiently redirected toward the new path. In this case, the other Floquet harmonics are only weakly excited (attributable to the discretization of the phase pattern on the surface), and our results indicate over 94% coupling efficiency in this example and more than 80% efficiency over an angular spectrum of 125°. Figure 3(c) shows the far-field scattering pattern for metasurfaces designed to deflect a plane wave at normal incidence into 41° (blue) and 63° (red) with a finite transverse length of 20 L; both cases exhibit ∼15-dB sidelobe level ratio, which confirms the excellent wave manipulation properties of the proposed optical meta-reflectarray, far superior to a conventional grating. The conversion efficiency and scattering directivity may be improved near grazing angles by utilizing a more refined phase discretization.

Along with their remarkable coupling efficiencies, the proposed meta-reflectarrays show surprisingly broad bandwidths of operation. To analyze their frequency response, it is relevant to realize that this proposed design is still a periodic structure in terms of its superlattice period; therefore, the incident plane
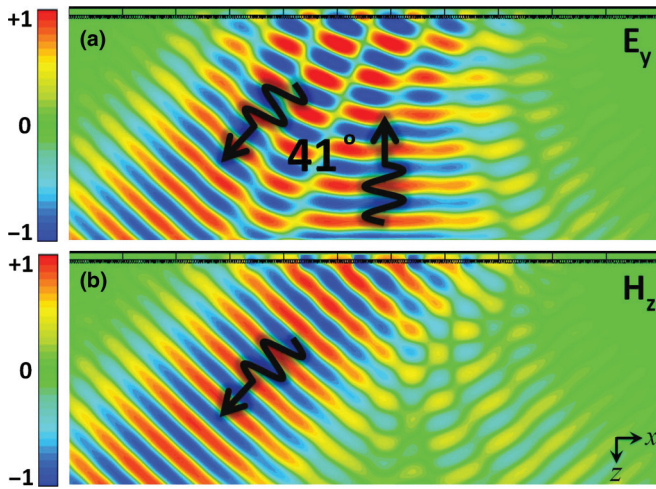
FIG. 4. (Color online) Beam manipulation. (a) Electric field and (b) magnetic field distribution (snapshot in time) under normal incidence for a finite length of the geometry in Fig. 1(b), illuminated with a Gaussian beam. Fields are plotted in the transverse plane (xz plane) to demonstrate efficient beam steering.

wave may couple to all propagating higher-order Floquet harmonics, as shown in Fig. 3(d). As we move away from the design frequency, the local dispersion of surface reactance may disturb the imprinted phase pattern and eventually decrease the coupling efficiency to the desired diffraction order. However, the proposed LC phase elements have an interesting dispersion response on their own, which allows sustaining moderately broadband performance: while the permittivity of materials (both plasmonic and dielectric) typically decreases toward shorter wavelengths, the effective local impedance holds a flat response because $Z_{\text{eff}} \propto (\omega(\varepsilon_p + \varepsilon_d))^{-1}$. This implies that the residual phase variation maintains a linear shape, as shown in Fig. 2(d), keeping the imparted transverse momentum almost constant as frequency changes. This is quite remarkable in ensuring that our design is inherently broadband. Figure 3(d) shows the distribution of the reflected power between different modes for the first metasurface design [Fig. 3(a)–3(b)].

The center design frequency is 600 THz, and the red curve indicates normalized power reflected toward the desired direction. The highlighted region shows a reasonable −3-dB bandwidth of operation, extended between 540 − 705 THz (420 − 560 nm). We need to stress that even though the meta-reflectarray is inherently broadband, the reflection angle shifts in frequency, due to the dispersion of the corresponding Floquet harmonic. This effect may be used to our advantage to realize efficient, ultrathin, and broadband planar optical spectrometers.

C. Optical wave manipulation

Beam steering is only one potential application in which the proposed meta-reflectarray concept may be useful. In its most general implementation, metasurfaces may be used to manipulate arbitrary wave fronts and not just plane waves. This would require that the building blocks constituting our design provide a robust angular response. Equation (2) actually suggests that this is the case, as long as the structure is electrically thin and with a small footprint, and such a condition indeed ensures good performance of metasurfaces for arbitrary beam manipulation. In this regard, Fig. 4 shows the full-wave simulation of a realistic finite-size metasurface reflector, designed to steer a normally incident Gaussian beam by 41° in reflection. Simulations confirm that the emerging phase front preserves the original distribution with a large conversion efficiency.

This approach may be used for various nanoscale applications. We envision, for instance, a flat optical lens that can focus the impinging wave at a desired distance. The required reflection phase follows a quadratic distribution, as shown in Fig. 5(a), forming an ultrathin flat mirror lens. Such a focusing low-profile plate may offer a variety of applications in optical microscopy and imaging and is directly integrable into nanophotonic systems with significant advantages compared to other proposed solutions at lower frequencies in terms of design, scalability, low profile, large numerical aperture, and full-phase coverage [18,39,41,42]. The simulated electric field and power distribution are shown in Fig. 5, where the meta-reflectarray forms a lens with focal distance set at $2\lambda_0$ and numerical aperture equal to NA = 0.9. The focusing
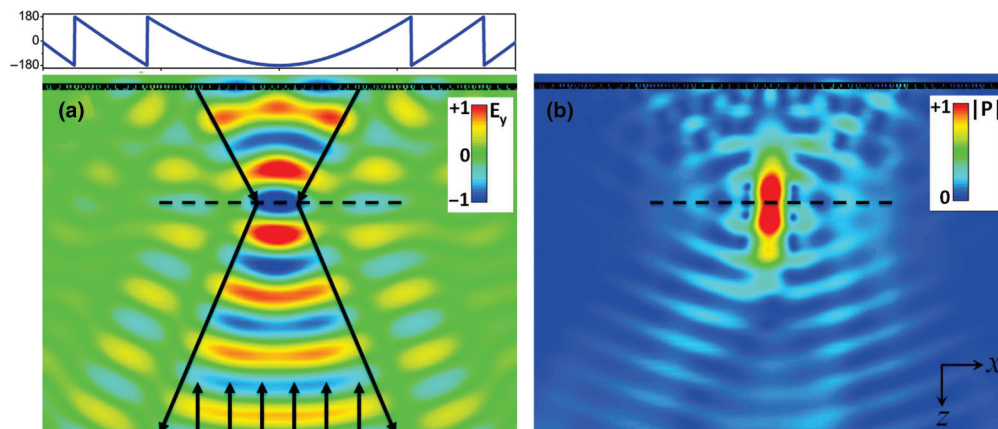

FIG. 5. (Color online) Beam collimation. (a) Electric field distribution (snapshot in time) and (b) power flow density for a metasurface designed at $\lambda_0 = 500$ nm to focus an impinging beam. The focal length of the lens is set at $2\lambda_0$ (indicated by the dashed horizontal lines) with numerical aperture NA = 0.9. The quadratic phase function imprinted on the surface is shown in (a), top panel.
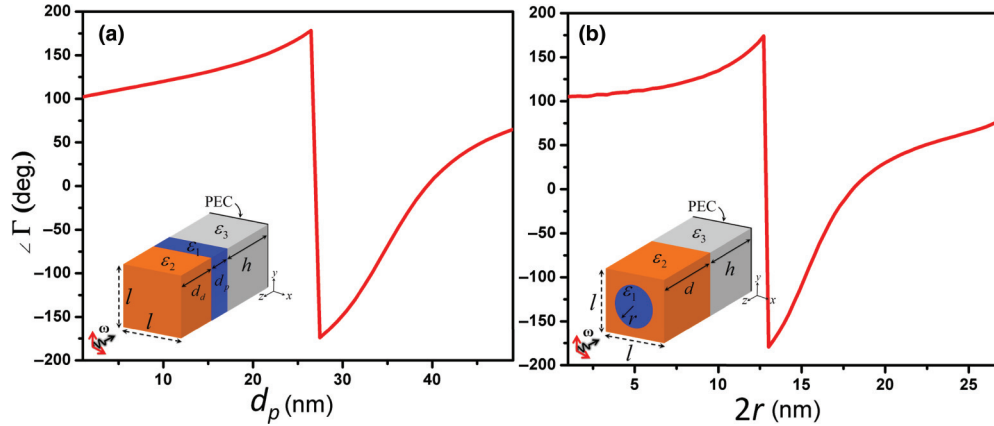
FIG. 6. (Color online) Polarization management. (a) Reflection phase variation for 2D periodic metasurfaces composed of the unit cell shown in the inset as a function of thickness d_p of the plasmonic segment. Dimensions are set at $h = 50$ nm, $d = d_d + d_p = 50$ nm, and $l = 31.25$ nm. The phase is calculated at $\lambda_0 = 500$ nm using full-wave numerical simulation, and the permittivities of constitutive materials are $\varepsilon_1 \approx (-8.14 - 0.095 j)\varepsilon_0$ (silver), $\varepsilon_2 = 12\varepsilon_0$ (aluminum arsenide), and $\varepsilon_3 = \varepsilon_0$ at the center frequency. (b) Same as in (a) for the concentric nanoblock shown in the inset. Dimensions are set at $h = 100$ nm, $d = 40$ nm, and $l = 31.25$ nm; the diameter of the nanorods are changed to span the entire phase spectrum. All phases are calculated at a plane 300 nm above the metasurface.

capability of the lens is robust to changes in frequency, thanks to its broadband functionality. With the full control over the phase resolution, the focal point may be placed at an arbitrary distance from the surface of the lens.

Along with static wave manipulation analyzed up to this point, a crucial feature of these metasurfaces is the possibility to add dynamic tunability to the design. Various choices may be explored, particularly regarding material properties, to enable real-time controllability of infrared and optical devices. Electromagnetic properties of the metasurface constitutive materials may be tuned by changing temperature (e.g., in vanadium dioxide), external bias (in semiconductor oxides), and/or via optical nonlinear effects, which may, furthermore, enable switching as an appealing trait at optical frequencies [10,43]. Our design principles, such as the phase maps in Fig. 2, may guide the real-time tunability of these elements in simple configurations.

D. Polarization management and influence of loss

The concept of deeply subwavelength phase modulation based on properly designed nanocircuit elements has been shown in the previous sections to provide several beneficial features. It is remarkable that our approach provides the freedom to operate with strong polarization preference or, on the contrary, realize metasurfaces that work for all polarizations of the incident wave. For instance, the basic phase element introduced in Fig. 1(a) was proposed as a 2D element, which acts as a parallel LC resonator for waves polarized along the nanorods. On the other hand, if we rotate the excitation by 90°, the surface operates as a series resonator (with new effective components), which shows weak phase dependence versus the filling ratio. This property implies that the metasurfaces analyzed in the previous sections can imprint totally different phase patterns on different incident polarizations. While it may deflect the parallel polarized field toward the desired direction, it imparts a conventional Snell reflection to the perpendicular polarization, providing an

interesting configuration for ultrathin polarization splitters or polarization cameras. In other scenarios, it may be of interest to realize more isotropic and polarization-independent devices. The concept of optical nanocircuits can be applied again in this context: it is possible to consider 3D elements, such as the ones shown in Fig. 6 (inset), in such a way to realize polarization-independent building blocks with similar phase control features. We used numerical full-wave simulations [40] in Fig. 6 to show that these structures are able to cover almost the entire 2π range by changing the filling ratio of the plasmonic portion over a lateral dimension of $l = \lambda_0/16$.

Another important issue is the robustness to losses, particularly important at optical frequencies, for which plasmonic metals are typically characterized by non-negligible losses. Also in this regard, our proposed metasurface concept provides a robust performance. Given the broadband response of our devices, in fact, the effect of loss is not significantly detrimental in any of the studied configurations, as we have verified with full-wave simulations. Indeed, all results presented in this paper include realistic silver loss in the metasurface elements. Simulations confirm that less than 6% of the input power is typically absorbed by the metasurface [see, e.g., Fig. 3(d)], and due to the low field concentration at the back mirror, the finite conductivity of a realistic metal in the ground plane only increases the absorption to a total of 8%. A consistent response is also obtained using more lossy plasmonic metals, such as gold, and our simulations confirm that the performance is not drastically affected by loss.

III. CONCLUSIONS

We have proposed here the concept and potential applications of ultrathin optical nanoresonators for the fast and efficient design of optical meta-reflectarrays. We have shown that carefully designed conjoined optical nanoblocks can operate as deeply subwavelength and scalable spatial phase modulators, drastically increasing the achievable resolution in wave manipulation over a broad range of frequencies,

of most interest for graded optical metasurfaces. The proposed structure is feasible with conventional lithography techniques and may be realized following a convenient and fast analytical design tool. Light bending, beam steering, and energy collimation have been demonstrated using these components, opening exciting venues to translate various powerful solutions available at radio frequencies to nanoscale optical devices. Additional features, such as tunability, may be envisioned in this configuration by controlling the material properties with temperature, bias, or by means of nonlinear effects. Our findings may be employed wherever efficient wave manipulation at the nanoscale is necessary, including signal processing [44], energy harvesting, holography, and the realization of compact integrated nanodevices.

[1] D. Smith, J. Pendry, and M. Wiltshire, Science **305**, 788 (2004).

[2] N. Engheta and R. W. Ziolkowski, *Metamaterials: Physics and Engineering Explorations*. (John Wiley & Sons, New York, 2006).

[3] A. B. Shvartsburg and A. A. Maradudin, *Waves in Gradient Metamaterials* (World Scientific Publishing Company, Singapore, 2013).

[4] R. A. Shelby, D. R. Smith, and S. Schultz, Science **292**, 77 (2001).

[5] V. M. Shalaev, Nature Photonics **1**, 41 (2007).

[6] Z. Liu, H. Lee, Y. Xiong, C. Sun, and X. Zhang, Science **315**, 1686 (2007).

[7] M. G. Silveirinha, A. Alù, and N. Engheta, Phys. Rev. E **75**, 036603 (2007).

[8] W. Cai, U. K. Chettiar, A. V. Kildishev, and V. M. Shalaev, Nat. Photonics **1**, 224 (2007).

[9] C. M. Soukoulis and M. Wegener, Nat. Photonics **5**, 523 (2011).

[10] A. V. Kildishev, A. Boltasseva, and V. M. Shalaev, Science **339**, 1289 (2013).

[11] N. Yu and F. Capasso, Nat. Mater. **13**, 139 (2014).

[12] Y. Zhao and A. Alù, Nano Lett. **13**, 1086 (2013).

[13] C. L. Holloway, E. F. Kuester, J. A. Gordon, J. O'Hara, J. Booth, and D. R. Smith, IEEE Antennas Propag. Mag. **54**, 10 (2012).

[14] N. Yu, P. Genevet, M. A. Kats, F. Aieta, J.-P. Tetienne, F. Capasso, and Z. Gaburro, Science **334**, 333 (2011).

[15] X. Ni, N. K. Emani, A. V. Kildishev, A. Boltasseva, and V. M. Shalaev, Science **335**, 427 (2012).

[16] F. Aieta, P. Genevet, N. Yu, M. A. Kats, Z. Gaburro, and F. Capasso, Nano Lett. **12**, 1702 (2012).

[17] S. Larouche and D. R. Smith, Opt. Lett. **37**, 2391 (2012).

[18] F. Aieta, P. Genevet, M. A. Kats, N. Yu, R. Blanchard, Z. Gaburro, and F. Capasso, Nano Lett. **12**, 4932 (2012).

[19] N. Engheta, A. Salandrino, and A. Alù, Phys. Rev. Lett. **95**, 095504 (2005).

[20] B. A. Munk, *Frequency Selective Surfaces: Theory and Design* (John Wiley & Sons, New York, 2005).

[21] S. Sun, K.-Y. Yang, C.-M. Wang, T.-K. Juan, W. T. Chen, C. Y. Liao, Q. He, S. Xiao, W.-T. Kung, and G.-Y. Guo, Nano Lett. **12**, 6223 (2012).

[22] F. Monticone, N. Mohammadi Estakhri, and A. Alù, Phys. Rev. Lett. **110**, 203903 (2013).

[23] C. Pfeiffer and A. Grbic, Phys. Rev. Lett. **110**, 197401 (2013).

[24] J. A. Encinar, IEEE Trans. Antennas Propag. **49**, 1403 (2001).

[25] M. E. Bialkowski and H. J. Song, IEEE Trans. Antennas Propag. **50**, 841 (2002).

[26] M. Chaharmir, J. Shaker, M. Cuhaci, and A. Ittipiboon, Microw. Opt. Technol. Lett. **48**, 1317 (2006).

[27] D. F. Sievenpiper, J. H. Schaffner, H. J. Song, R. Y. Loo, and G. Tangonan, IEEE Trans. Antennas Propag. **51**, 2713 (2003).

[28] Y. Sun, B. Edwards, A. Alù, and N. Engheta, Nat. Mater. **11**, 208 (2012).

[29] A. Alù and N. Engheta, Phys. Rev. Lett. **104**, 213902 (2010).

[30] A. Alù and N. Engheta, Nat. Photonics **2**, 307 (2008).

[31] A. Salandrino and N. Engheta, Phys. Rev. B **74**, 075103 (2006).

[32] A. Alù, M. E. Young, and N. Engheta, Phys. Rev. B **77**, 144107 (2008).

[33] A. Alù and N. Engheta, J. Opt. Soc. Am. B **23**, 571 (2006).

[34] N. Engheta, Science **317**, 1698 (2007).

[35] A. Alu and N. Engheta, Proc. IEEE **99**, 1669 (2011).

[36] This choice of center frequency is completely arbitrary here, and the general idea described in this paper is applicable in different regions of frequency. Proper plasmonic materials must be chosen for the preferred frequency of operation and target bandwidth, ranging from infrared to the visible spectrum. For example aluminum-doped zinc oxide semiconductors operate as plasmonic materials at infrared frequencies, while noble metals, such as silver and gold, may be employed at optical frequencies.

[37] S. Adachi, J. Appl. Phys. **58**, R1 (1985).

[38] M. A. Ordal, R. J. Bell, Jr. Alexander, R. L. Long, and M. Querry, Appl. Opt. **24**, 4493 (1985).

[39] A. Pors, M. G. Nielsen, R. L. Eriksen, and S. I. Bozhevolnyi, Nano Lett. **13**, 829 (2013).

[40] Computer Simulation Technology, CST Studio Suite 2012, http://www.CST.com.

[41] X. Li, S. Xiao, B. Cai, Q. He, T. J. Cui, and L. Zhou, Opt. Lett. **37**, 4940 (2012).

[42] D. Fattal, J. Li, Z. Peng, M. Fiorentino, and R. G. Beausoleil, Nat. Photonics **4**, 466 (2010).

[43] P.-Y. Chen and A. Alù, Phys. Rev. B **82**, 235405 (2010).

[44] A. Silva, F. Monticone, G. Castaldi, V. Galdi, A. Alù, and N. Engheta, Science **343**, 160 (2014).